A system for performing simultaneous *in situ* atomic force microscopy/optical microscopy measurements on electrode materials for lithium-ion batteries

L. Y. Beaulieu and V. K. Cumyn
Department of Physics, Dalhousie University, Halifax, Nova Scotia B3H 3J5, Canada

K. W. Eberman and L. J. Krause
3M Company, St.-Paul, Minnesota 55144-1000

J. R. Dahn[a)]
Department of Physics and Department of Chemistry, Dalhousie University, Halifax, Nova Scotia B3H 3J5, Canada

(Received 20 February 2001; accepted for publication 4 June 2001)

An atomic force microscope (AFM) equipped with an optical charge coupled device camera has been placed in an Ar filled glovebox for the purpose of studying the change in morphology of electrode materials as they react with lithium. In order to minimize noise induced by vibration, the AFM is mounted on granite blocks suspended from the ceiling of the glovebox by a combination of flexible rubber cords and metal springs. The AFM, which is equipped with an environmental chamber surrounding the sample, is then enclosed in a specially constructed draft shield that allows the circulation of Ar gas by the purification system during imaging. A special electrochemical cell was constructed to hold the working electrode under study. Repeated imaging with little drift is possible while electrodes are reacted with lithium for periods of many days. Examples of measurements made by this device will be given for the case of lithium alloying with sputter-deposited Si–Sn thin films. The optical and AFM images obtained as a function of lithium content in the films are assembled into time-lapsed ''movies'' showing the evolution of the morphology of the sample along with the corresponding electrochemistry. These movies are available for download through the Electronic Physics Auxiliary Publication Service (EPAPS).
 [DOI: 10.1063/1.1388214]

I. INTRODUCTION

In recent years there has been a great deal of research focused on using intermetallic compounds as anode materials for lithium-ion batteries.[1–7] Although intermetallic systems offer, in most cases, a large increase in both volumetric and gravimetric capacity, none have been able to match the capacity retention as a function of cycle number obtained by graphite. The reason why graphite is such a good electrode material is because its reversible reaction with lithium is an intercalation process that is very benign.[8] The reaction of lithium with metals like Sn, Si, Al, etc. is an alloying reaction and unlike intercalation, is not benign. As lithium reacts with such metals new intermetallic phases normally form[9] that have different crystal structures, and larger volume (up to four times larger for $Li_{4.4}Si$ compared to Si) than the original metal. In cases where the Li–metal phase diagram shows two-phase regions, inhomogeneous expansion results when two phases of different lithium content exist in the same particle. This is thought to lead to cracking and loss of electrical contact to the particles. However, the cracking of electrode particles can be eliminated if the expansions and contractions are homogeneous.[10] This can be achieved by eliminating the two-phase regions in the Li–M phase diagram, by using nanostructured materials.[10] Nevertheless, even if the expansions are homogeneous, they are still large. For example, the Si–Al and Si–Sn materials described in Ref. 11 are thought to approximately triple their volume as lithium is added to maximum composition. It is essential that such volume changes be measured and monitored. We are not aware of any previous studies of the morphology changes of electrode particles subjected to numerous reversible electrochemical reactions. This article describes a simultaneous

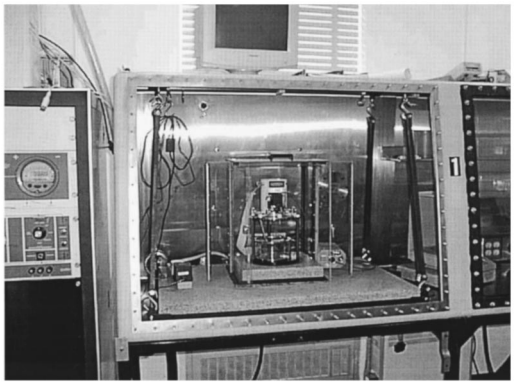

FIG. 1. The AFM inside the glovebox prior to closing the box.

a)Author to whom correspondence should be addressed; electronic mail: jeff.dahn@dal.ca

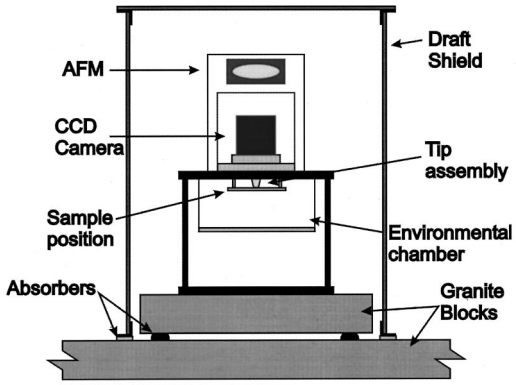

FIG. 2. Schematic representation of the AFM setup.

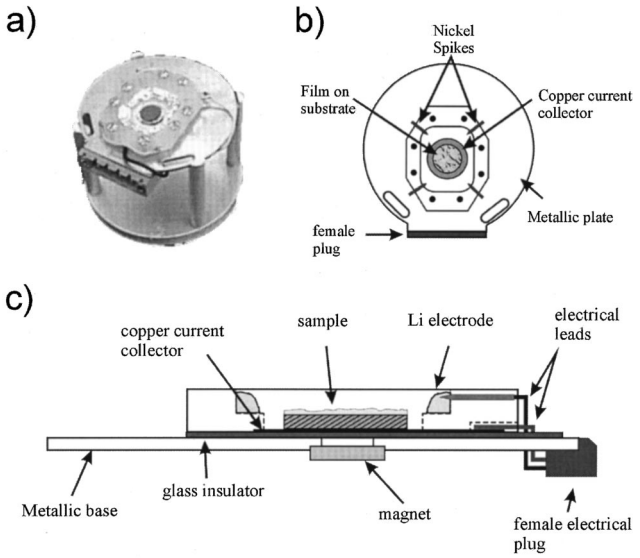

FIG. 3. (a) Photograph of the wet cell used in our studies. (b) Top view and (c) side view schematic representation of the wet cell used in our studies.

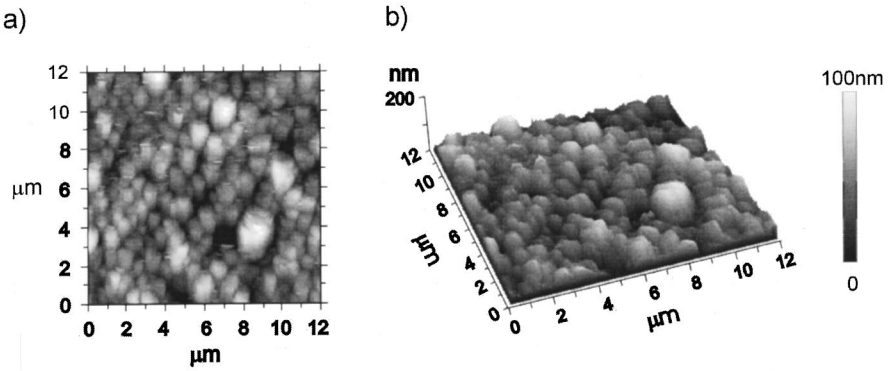

FIG. 4. Typical (a) two-dimensional and (b) three-dimensional AFM images of the surface of the Si–Sn thin film electrode materials studied herein.

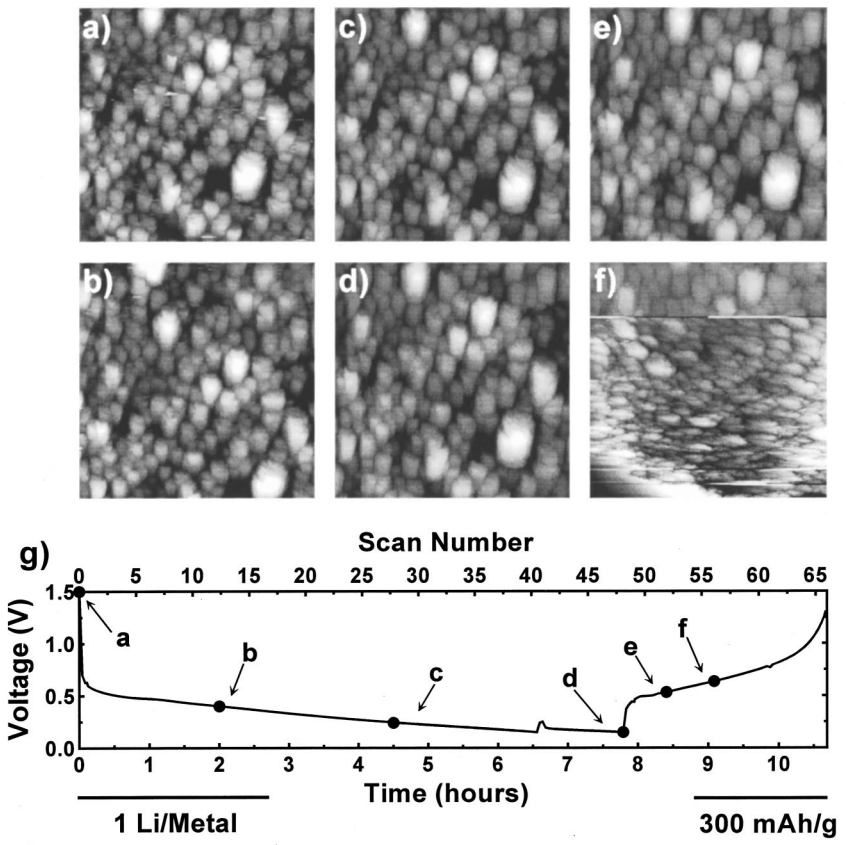

FIG. 5. Results of an *in situ* AFM experiment performed on a Si–Sn alloy film. The AFM images are all 12×12 μm in size. The contrast scale from dark to light corresponds to (a) 0–100, (b) 0–110, (c) 0–150, (d) 0–205, (e) 0–215, and (f) 0–330 nm. (g) The voltage vs time (bottom abscissa) and AFM scan number (top abscissa). The bars in (g) show, on the left, the time corresponding to 1 Li/metal at the current used and, on the right, the capacity scale in mAh/g.

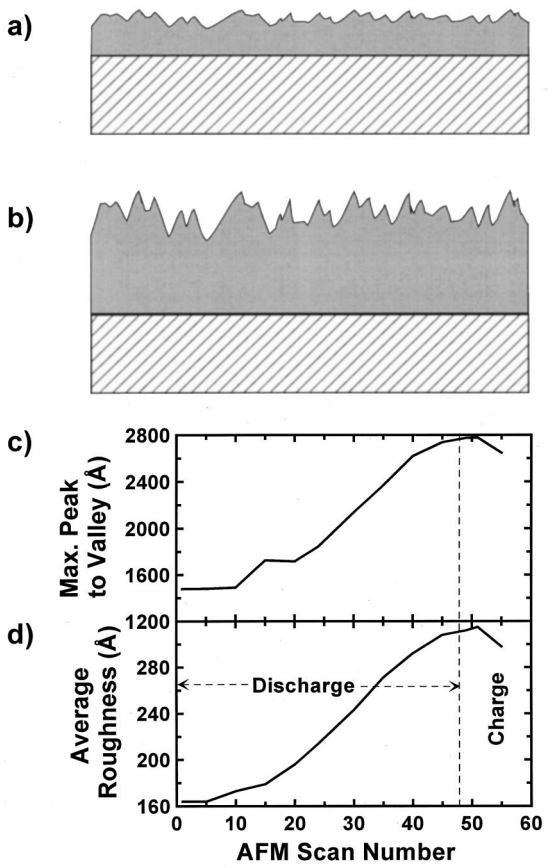

FIG. 6. (a) Schematic representation of the rough sample (dark gray) on a flat substrate (hashed area). (b) Effect on the roughness when the sample (dark gray) on a flat substrate (hash area) is doubled in sized. (c) The maximum peak to valley distance and (d) average roughness of the electrode surface obtained from a statistical analysis of the AFM images collected during the experiment highlighted in Fig. 5.

in situ atomic force microscopy (AFM)/optical microscopy system suited to these and other electrochemical studies.

In situ AFM and scanning tunneling microscopy have been used to study electrodeposition[12,13] and nickel hydroxide electrodes.[14,15] In particular, *in situ* AFM, has been used to study the formation of the solid electrolyte interphase on model surfaces like highly oriented pyrolytic graphite.[16] Recently a system has been constructed to perform *in situ* studies on electrochemical cells.[17,18] This system, although ingenious in its design, is very restrictive due to its small size. In this article we show how a scanning probe microscope (SPM) system can be incorporated into a full size double glovebox and used to study air sensitive materials. The advantages of using a large glovebox are numerous. Commercial gloveboxes equipped with purification systems allow for an inert atmosphere to be maintained for long periods of time. A full size glovebox allows the user a much better control of his/her equipment. Moreover, sample preparation and sample imaging are done in the same environment without any risk of contamination due to relocation.

II. EQUIPMENT

A Molecular Imaging (Pheonix, Arizona) PicoScan SPM with two AFM scanners (37×37 μm and 6×6 μm) was placed inside an argon-filled double glovebox [Vacuum Atmospheres (Hawthorne, California) equipped with a MO-40-1 V dry train] where the water and oxygen levels are kept below 1 ppm. The SPM system is equipped with a charge coupled device (CCD) optical camera that allows the user to view the sample in the area of the position of the cantilever of the nanoprobe.

All electrochemical tests were performed in a homemade electrochemical cell (herein called a wet cell) using ethylene carbonate/propylene carbonate [(EC/PC) 1:1 vol. EM science] electrolyte and lithium metal (FMC) as the negative electrode. This electrolyte was chosen since it has a very low vapor pressure that prevents it from evaporating from the open wet cell for weeks. Cells were cycled using constant discharge and charge currents using a computer controlled Keithley 236 source-measure unit.

The samples used in this study were made as described in Ref. 11. The substrates used were highly polished metal disks (400 series stainless steel, 1 cm in diameter and approximately 2.5 mm thick). In order to improve the adhesion between the active material and the substrate, an intermediate layer (approx. 4 μm thick) of copper was applied by sputtering. Prior to the application of copper the initial metal substrate was etched with an argon plasma to help remove any contaminants which might hinder adhesion. Once the copper layer was applied, the active material (1 μm thick) was immediately applied by sputtering.

III. EXPERIMENTAL SETUP

Figure 1 shows the glovebox, with the purifier system to the left, in which all experiments were conducted. The glovebox is connected to the dry-train by two 38 mm diameter (inner diameter) pipes which allow the circulation of Ar from the glovebox to the purifier. The interior of the glovebox is divided in 2. The right side of the glovebox, not shown in Fig. 1, is used for sample preparation while the left side of the glovebox is used to hold the AFM. The AFM sits on two granite slabs weighing 11 kg (small slab) and 70 kg (large slab) each. The large granite slab is suspended from the ceiling of the glovebox by a combination of two flexible rubber cords and one metal spring at each corner. The metal springs are used to support the large mass while the rubber cords are used as vibration dampers.

Figure 2 shows a schematic representation of the AFM setup inside the glovebox. The AFM sits centrally on the small granite slab that sits on rubber dampers that sit on the large granite slab. Because of the sensitivity of the AFM a draft shield was designed and constructed to allow for the continual circulation of argon gas inside the glovebox by the purification system. The draft shield rests on dampers that rest on the large granite slab. An environmental chamber below the AFM (also shown in Fig. 2) further isolates the sample. The CCD camera, represented by the black square, is used to optically monitor the topography of our samples to obtain information on the micron scale.

Figure 3(a) shows a picture of the wet cell used in our experiments. This picture shows the position of the sample as well as the lithium foil used as both the reference and

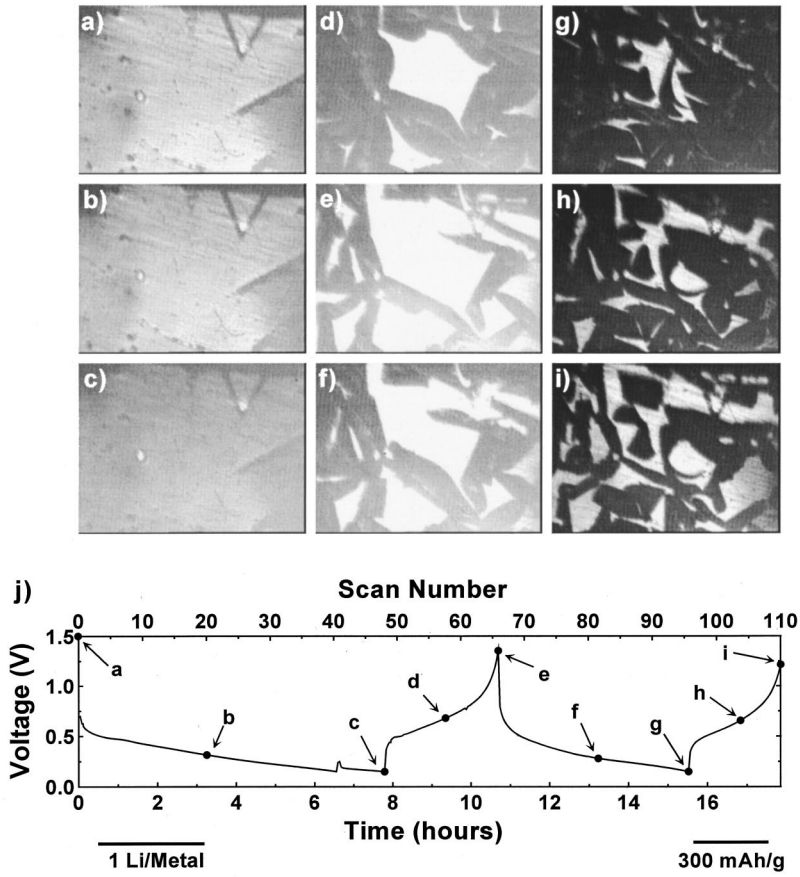

FIG. 7. Results of an *in situ* optical microscopy experiment performed on the same film as described by Figs. 4 and 5. The optical images (a)–(i) are approximately 1000×700 μm in size. (j) The voltage vs time (bottom abscissa) and AFM scan number (top abscissa). The bars in (j) show, on the left, the time corresponding to 1 Li/metal at the current used and, on the right, the capacity scale in mAh/g.

counter electrode. Figures 3(b) and 3(c) show schematic views of the construction of the wet cell. The sample sits on a copper current collector and is held in place by a rare earth magnet under the baseplate. The current collector is electrically isolated from the baseplate by a thin glass plate. This ensures that the AFM and the Keithley 236, used to control the cell, are electrically isolated. The Li metal electrode sits on a ledge in the polypropylene well and is cold welded onto four nickel spikes which protrude through the walls of the well. Wires from the copper current collector and the nickel spikes are fed to a female plug at the front of the wet cell. All electrical connections from the inside of the glovebox to the outside are made by a commercial airtight electrical feedthrough (not shown).

IV. EXPERIMENTAL RESULTS

Figure 4 shows an AFM image[19] of the surface of a Si–Sn[11] metallic film studied in our experiments. Figure 4(a) shows the two-dimensional AFM image of a 12×12 μm portion of the electrode surface. The color scheme from black to white corresponds to 0–100 nm as shown by the scale bar on the right. Figure 4(b) shows a three-dimensional representation of the same portion of the surface. As can more clearly be seen, the surface is corrugated on the nanometer scale.

Figure 5 shows the results of an *in situ* AFM experiment[20] conducted on the electrode shown in Fig. 4. The cell voltage is plotted versus time (bottom abscissa) and AFM scan number (top abscissa) in Fig. 5(g). The indicated points on the voltage curve show the points during the discharge (or charge) to which the AFM images [Figs. 5(a)–5(f)] correspond. A scale bar at the lower left indicates the time corresponding to 1 Li/metal and the scale bar at the lower right indicates the capacity scale in mAh/g. Note that 1900 mAh/g corresponds to 4.4 Li atoms per metal atom for this film. Figures 5(a)–5(d) show the evolution of the morphology of the film as it reacts with lithium during the first discharge. The charge cycle (removing lithium) of this experiment shows different results than those obtained for the discharge cycle due to poor adhesion between the metallic film and the substrate. This is seen by the loss of the AFM image as shown in Fig. 5(f) midway during the first charge cycle. The poor adhesion of this film can be seen more clearly from the optical images taken simultaneously.

Figures 5(a)–5(d) suggest that the insertion of lithium into the metal film during the first discharge causes virtually no change to the surface morphology. However, the vertical distance corresponding to maximum contrast (white to black) increases from (a) to (d) showing a proportional increase in corrugation with film thickness. The top panels of Fig. 6 show a sketch of an initially rough film, on a flat substrate, that then doubles in thickness everywhere (much like the thickness change of an electrode material after incorporation of lithium). Notice that the corrugation also doubles which implies that the thickness change suffered by the electrode can be obtained from the change in roughness.[21] The increase in corrugation of the electrode surface is best described by comparing the change in the average roughness (mean absolute deviation from the average film height) with

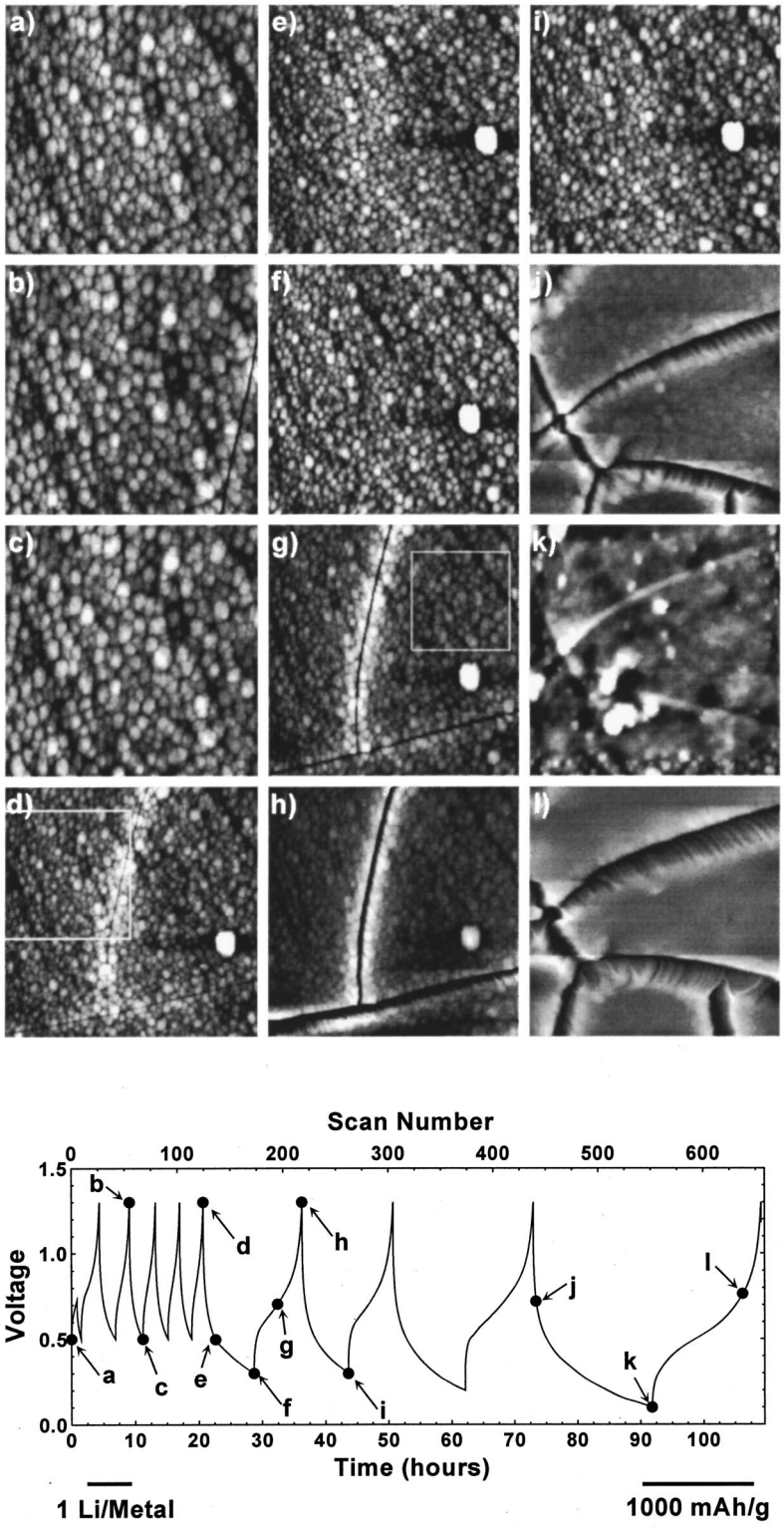

FIG. 8. Results of an *in situ* AFM experiment performed on an intermetallic film. The AFM images (a)–(c) are 19×19 μm and the AFM images (d)–(l) are 37×37 μm in size. The contrast scale from dark to light corresponds to (a) 0–150, (b) 0–138, (c) 0–140, (d) 0–185, (e) 0–150, (f) 0–185, (g) 0–270, (h) 0–440, (i) 0–175, (j) 0–1040, (k) 0–290, and (l) 0–1900 nm. (m) The voltage vs time (bottom abscissa) and AFM scan number (top abscissa). The bar in (m) shows the time corresponding to 1 Li/metal at the current used.

lithium content. The lower panels of Fig. 6 show the average roughness and the maximum peak to valley distance versus lithium content for images collected during the experiment described by Fig. 5. Both the maximum peak to valley distance and the average roughness increase, as expected, with the insertion of lithium into the electrode.

It is not possible to make quantitative measurements of the volume expansion of the film based on roughness changes alone, unless the substrate on which the film is deposited has a roughness itself that is negligible compared to that of the roughness of the film on the substrate. The average roughness of our polished stainless steel substrates is about 80 Å (average of measurements over three substrates), only a factor of 2 smaller than that of the sputtered film. Furthermore, we did not measure the roughness of the surface after the deposition of the 4-μm-thick copper layer. Since the alloy film is deposited on an initially rough surface, the original roughness of the alloy film has a contribution

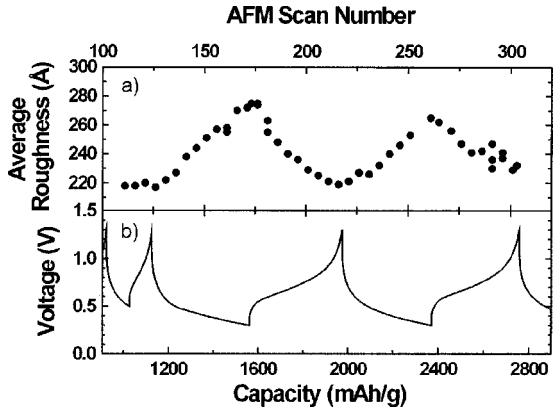

FIG. 9. The (a) average roughness and (b) voltage as a function of capacity (bottom abscissa) and AFM scan number (top abscissa) of the electrode surface obtained from a statistical analysis of the AFM images collected during the experiment highlighted in Fig. 8.

from the underlying material. This contribution does not change, as the thickness of the alloy film changes, so the fractional roughness change measured at the alloy surface will be less than if the film had been deposited on a perfectly flat substrate. Therefore, although the average roughness doubles as lithium is inserted into electrode as shown in Fig. 6, we can only conclude that the volume expansion is at least double.

Figure 7 shows optical images recorded[22] at the same time as the AFM images shown in Fig. 5. In this case the reaction of lithium with the electrode is shown over two full discharge/charge cycles. The integrity of the metallic film collapses midway during the first charge cycle. This is because the adhesion between the film and the substrate is not strong enough to withstand the tensile stress in the film as the lithium atoms are removed. During the first charge cycle, removing lithium causes the film to crack, as shown in Fig. 7(d), and become disconnected from the substrate everywhere except for a very small area where the electrical contact is maintained. Continual removal of lithium then causes the film to curl as seen in Fig. 7(e). Reinserting lithium into the film as shown in Figs. 7(f) and 7(g) causes the particles to expand and return almost to their original state. Figures 7(h) and 7(i) show the same trend as displayed in Figs. 7(d) and 7(e) during the removal of lithium from the electrode. Different strategies have been employed to improve the adhesion between the film and the substrate during the cycling process. The next example illustrates what happens to a metallic film when it remains better adhered to the substrate.

Figure 8 shows the results of an *in situ* AFM experiment conducted on a Si–Sn^{11} metallic film.[23] The voltage versus time (bottom abscissa) and AFM scan number (top abscissa) shows the electrochemical results for nine discharge/charge cycles. Notice that continuous AFM scanning for 120 h was possible. A scale bar at the lower left indicates the time corresponding to 1 Li/metal and the scale bar at the lower right indicates the capacity scale in mAh/g. Figures 8(a) to 8(l) show the AFM images taken *in situ*. Images (a), (b), and (c) are 19×19 μm in size and images (d)–(l) are 37×37 μm in size. The location of the scan area of images (a), (b), and (c) is partially shown in Fig. 8(d) by the white square frame. The AFM image in Fig. 8(a) shows the morphology of the electrode at scan 0. The vertical contrast scale for this image from black to white corresponds to 0–150 nm. The surface roughness of the initial electrode is approximately 220 Å which is typical for these films. Figure 8(b) shows the surface of the electrode after lithium has been completely removed. The crack shown in the lower left corner shows the results of the contraction undergone by the electrode during delithiation. Reinserting lithium into the electrode causes the film to expand, thereby closing the crack. This can be seen in Fig. 8(c) where no trace of the crack is observed. Looking at a larger scan area, Fig. 8(d) shows the same results as Fig. 8(b). This time two cracks are observed. More importantly, this image shows by comparison to image 8(b), the initial crack pattern formed during the first charge cycle is preserved in later cycles. Figures 8(e) and 8(f) show that the cracks close as lithium is reinserted into the film and the electrode particles expand. During the portion of the voltage profile between (e) and (f), more lithium is allowed to react with the film causing a greater expansion then in the previous discharge/charge cycles. Since the film has now suffered a greater expansion, removing the lithium as shown in Figs. 8(g) and 8(h) causes the cracks to become larger and more pronounced. The contrast scale of image 8(h) corresponds (from dark to light) to 0–440 nm, respectively, which is much larger than that of image 8(d) (0–185 nm from dark to light). Figure 8(h) also shows the how the crack edges are beginning to curl and lift from the substrate. As seen in Fig. 8(i), reinserting lithium into the electrode shows once again how the expansion of the electrode causes the cracks to close and the electrode to flatten.

The last three AFM images shown in Figs. 8(j), 8(k), and 8(l) show the change in morphology of the electrode surface when the electrode is made to react with an even larger amount of lithium. Although these images were taken at a slightly different area on the electrode, the effect of the increased addition and removal of lithium is clear by the increase in the size of the cracks shown in images 8(j) and 8(l).

A statistical analysis was performed on the AFM images obtained in the experiment shown in Fig. 8. Because the interest of this analysis was to monitor the change in morphology of the portions of the film which remain adhered to the substrate, the analysis was conducted in the area highlighted in Fig. 8(g) by the white frame. Figure 9 shows the change in the average roughness [9(a)] of the highlighted area compared to the voltage curve collected during the experiment [9(b)]. As discussed previously, the insertion of lithium in the electrode causes the latter to expand vertically which in turn creates a commensurate increase in roughness. The roughness changes are exactly correlated to the switch points from discharge (adding lithium) to charge (removing lithium).

ACKNOWLEDGMENTS

The authors thank the Natural Science and Engineering Research Council of Canada and 3M Canada Inc. for financial support of this work under the Industrial Research Chair and Research Grant programs.

[1] B. A. Boukamp, G. C. Lesh, and R. A. Huggins, J. Electrochem. Soc. **128**, 725 (1981).
[2] J. Wang, I. D. Raistrick, and R. A. Huggings, J. Electrochem. Soc. **133**, 457 (1986).
[3] A. A. Anani, S. Crouch-Baker, and R. A. Huggings, J. Electrochem. Soc. **135**, 2103 (1988).
[4] J. Yang, M. Winter, and J. O. Besenhard, Solid State Ionics **90**, 281 (1996).
[5] Y. Idota, A. Matsufuji, Y. Maekawa, and T. Miyasaka, Science **276**, 1395 (1997).
[6] Ou Mao, R. A. Dunlap, and J. R. Dahn, J. Electrochem. Soc. **146**, 2 (1999).
[7] L. Y. Beaulieu, D. Larcher, R. A. Dunlap, and J. R. Dahn, J. Electrochem. Soc. **147**, 9 (2000).
[8] *Intercalation Chemistry*, edited by M. S. Whittingham and A. J. Jacobson (Academic, New York, 1990).
[9] W. G. Moffat, *Handbook of Binary Phase Diagrams* (Genium, Schenectady, 1990).
[10] O. Mao, R. L. Turner, I. A. Courtney, B. D. Fredericksen, M. I. Buckett, L. J. Krause, and J. R. Dahn, Electrochem. Solid-State Lett. **2**, 1 (1999).
[11] R. L. Turner, World Intellectual Property Organization Patent Application WO 00/03444 (2000).
[12] Q. Wu and D. Barkey, J. Electrochem. Soc. **144**, 9 (1997).
[13] C. J. Weber, H. W. Pickering, and K. C. Weil, J. Electrochem. Soc. **144**, 7 (1997).
[14] P. Häring and R. Kötz, J. Electroanal. Chem. **385**, 273 (1995).
[15] A. Kowal, R. Niewiara, B. Perończyk, and J. Haber, Langmuir **12**, 2332 (1996).
[16] K. Edström and M. Herranen, J. Electrochem. Soc. **147**, 10 (2000).
[17] Y. Cohen and D. Aurbach, Rev. Sci. Instrum. **70**, 12 (1999).
[18] D. Aurbach and Y. Cohen, J. Electrochem. Soc. **2**, 1 (1999).
[19] All AFM images shown in this article were taken by constant force contact mode.
[20] See EPAPS Document No. E-RSINAK-72-003109 for Movie1 showing the reaction of lithium with this electrode. This document may be retrieved via the EPAPS homepage (http://www.aip.org/pubservs/epaps.html) or from ftp.aip.org in the directory /epaps/. See the EPAPS homepage for more information.
[21] L. Y. Beaulieu, A. D. Rutenberg, and J. R. Dahn, Microsc. Microanal. (submitted).
[22] See EPAPS Document No. E-RSINAK-72-003109 for Movie2 showing the complete reaction of lithium with this electrode. This document may be retrieved via the EPAPS homepage (http://www.aip.org/pubservs/epaps.html) or from ftp.aip.org in the directory /epaps/. See the EPAPS homepage for more information.
[23] See EPAPS Document No. E-RSINAK-72-003109 for Movie3 showing the complete reaction of lithium with this electrode. This document may be retrieved via the EPAPS homepage (http://www.aip.org/pubservs/epaps.html) or from ftp.aip.org in the directory /epaps/. See the EPAPS homepage for more information.